THE ASTROPHYSICAL JOURNAL, 588:674–679, 2003 May 10

STRUCTURE OF DARK MATTER HALOS FROM HIERARCHICAL CLUSTERING. II. DEPENDENCE OF COSMOLOGICAL MODELS IN CLUSTER-SIZED HALOS

TOSHIYUKI FUKUSHIGE
Department of General Systems Studies, College of Arts and Sciences, University of Tokyo, 3-8-1 Komaba, Meguro-ku, Tokyo 153-8902, Japan
AND
JUNICHIRO MAKINO
Department of Astronomy, School of Sciences, University of Tokyo, 7-3-1 Hongo, Bunkyo-ku, Tokyo 117-0033, Japan
Received 2001 August 1; accepted 2003 January 15

ABSTRACT

We investigate the structure of the dark matter halos formed in three different cold dark matter scenarios using *N*-body simulations of 13 cluster-sized halos. With the resolution of our simulations, the density profile is reliable down to ~1% of the virial radius. In all runs, density cusps proportional to $r^{-1.5}$ developed down to the reliable limit. This result was independent of the cosmological models we simulated. We could not reproduce the cusp shallower than $r^{-1.5}$, which was obtained in some previous studies.

Subject headings: cosmology: theory — dark matter — galaxies: clusters: general — methods: *n*-body simulations

1. INTRODUCTION

The structure of dark matter halos formed through dissipationless hierarchical clustering from a cosmological initial setting has been explored by many researchers since the "finding" of the universal profile by Navarro, Frenk, & White (1996, 1997, hereafter NFW). NFW performed *N*-body simulations of the halo formation and found that the density profiles of dark matter halos were expressed well by a simple formula,

$$\rho_{\rm NFW} = \frac{\rho_0}{(r/r_0)(1+r/r_0)^2} \ , \qquad (1)$$

where ρ_0 is a characteristic density and r_0 is a scale radius. They argued that the profile of dark matter halos have the same shape, independent of the halo mass, the initial density fluctuation spectrum, or the value of the cosmological parameters.

Although the NFW results have been confirmed regarding the logarithmic slope shallower than isothermal near the center and -3 in the outskirts, disagreements concerning the slope of the central region were reported by subsequent studies in which higher resolution simulations were performed. The disagreements are summarized into the following two kinds:

1. One is that the slope at the center is steeper than that in the NFW result. Fukushige & Makino (1997, hereafter FM97) performed a simulation with 768k particles, while previous studies employed ~20k and found that the galaxy-sized halo in their simulation has a cusp steeper than $\rho \propto r^{-1}$. Moore et al. (1998, 1999, hereafter M99) and Ghigna et al. (2000) performed simulations with up to 4M particles and obtained the results that the profile has a cusp proportional to $r^{-1.5}$ in both galaxy-sized and cluster-sized halos. They proposed the modified universal profile (hereafter the M99 profile),

$$\rho_{\rm M99} = \frac{\rho_0}{(r/r_0)^{1.5}\left[1+(r/r_0)^{1.5}\right]} \ . \qquad (2)$$

Klypin et al. (2001) also obtained the results that show that the slope at the center can be approximated by $r^{-1.5}$, although they argued that the NFW fit is still good up to their resolution limit.

2. The second is that the slope at the center is not universal. Jing & Suto (2000) performed a series of *N*-body simulations and concluded that the power of the cusp depends on mass, in contradiction to the claims by earlier studies. It varies from -1.5 for the galaxy-mass halo to -1.1 for the cluster-mass halo. Also, many analytical studies argued that the halo profile should depend on the power spectrum of the initial density fluctuation. For example, Hoffman & Shaham (1985) and Syer & White (1998) predicted the slopes $3(n+3)/(n+4)$ and $3(n+3)/(n+5)$, respectively, where n is the effective power-law index of the power spectrum.

In the first paper of this series (Fukushige & Makino 2001, hereafter Paper I), we performed simulations of 12 halos with masses ranging from 6.6×10^{11} to 8.0×10^{14} $M_\odot$. We found that, in all runs, the halos have density cusps proportional to $r^{-1.5}$ developed at the center. This result means that the density structure is universal in the sense that it is independent of the halo mass.

This paper is a follow-up to Paper I. In this paper, we focus on the dependence of the halo profile on the cosmological model. We simulate halos in three conventional cold dark matter models: standard, lambda, and open CDM models, while simulations in Paper I was performed only in the standard CDM model. We performed *N*-body simulations of formation of 13 cluster-sized dark matter halos using the Barnes-Hut tree code and a special-purpose computer GRAPE-5 (Kawai et al. 2000). The goal of the original NFW paper was to investigate the dependence of the structure of CDM halos on different cosmological models. As has been demonstrated by many follow-up works discussed above, its resolution was not high enough to determine the central slope accurately. This lack of the resolution was also the case for similar works (Thomas et al. 1998; Huss, Jain, & Steinmetz 1999). In the present paper we provide, for the first time, the result of numerical simulations

TABLE 1
COSMOLOGICAL MODELS

Model	Ω_0	λ_0	h	σ_8	z_i
SCDM	1.0	0.0	0.5	0.6	24.0
LCDM.....	0.3	0.7	0.7	1.0	32.3
OCDM	0.3	0.0	0.7	1.0	32.3

from a wide range of cosmological models, with resolution high enough to determine the slope of the central cusp reliably.

The structure of this paper is as follows. In § 2, we describe the model of our N-body simulation. In § 3, we present the results of the simulation. Section 4 is for conclusion and discussion.

2. SIMULATION METHOD

We simulated the formation of the dark matter halos using "resimulation" method, which has been the standard method for the simulation of halo formation since NFW. In this method, we first perform large-scale cosmological simulations in order to identify the halo candidates. We trace back to the initial condition of the large-scale simulation and express the halo candidate with a larger number of particles by adding a shorter wavelength perturbation. Then we resimulate the halo candidates.

We used three cosmological models listed in Table 1: standard, open, and lambda cold dark matter models (SCDM, OCDM, and LCDM). Here, Ω_0 is the density parameter, λ_0 is the dimensionless cosmological constant, $H_0 = 100\ h$ km s^{-1} Mpc^{-1} at the present epoch, and z_i is the initial redshift. The amplitudes of the power spectrum in CDM models were normalized using the top-hat–filtered mass variance at 8 h^{-1} Mpc according to the cluster abundance (Kitayama & Suto 1997).

The large-scale cosmological simulations were performed with 1.1×10^6 particles in a sphere of 100 Mpc radius. The procedure for setting the initial condition were the same as those used in Fukushige & Suto (2001). We regard a spherical overdensity region around a local potential minimum within r_v as a candidate halo. We define the radius r_v such that the spherical overdensity inside is $178\Omega_0^{0.3}$ times the critical density for the SCDM and OCDM models and $178\Omega_0^{0.4}$ times for the LCDM model (Eke, Cole, & Frenk 1996).

We selected 13 halos from the candidate halos catalog, which are summarized in Table 2. We first selected the most massive halo in each CDM model and then selected the halos at random from halo candidates containing more than 1000 particles. We expressed a region within $5r_v$ from the center of the halo at $z = 0$ in the cosmological simulation with a larger number of particles. We placed particles whose mass is the same as that in the cosmological simulation in a sphere of $\sim$50 Mpc radius surrounding the high-resolution region in order to express the external tidal field. The total number of particles, N, is listed in Table 2. As a result, the mass ratio between the high-resolution particles and surrounding particles becomes rather large, 256–2048. In order to prevent the contamination of heavy particles into the halo, we set the boundary to be a rather large value, $5r_v$. No heavy particle entered within r_v throughout all simulations.

We integrated the system directly in the physical coordinates for both the cosmological and halo simulations (as in FM97; Paper I). We used a leap-frog integrator with shared and constant time step. The step size for the cosmological simulation is $\Delta t/t_H = 1/1024$, and that for the halo simulation is listed in Table 2. The code for the time integration is the same as that in Fukushige & Suto (2001). We used the usual Plummer softening. The gravitational softening ϵ is constant in the physical coordinates, and the length is 5 kpc for the cosmological simulation and 1 kpc for all halo simulations.

The force calculation is done with the Barnes-Hut tree code (Barnes & Hut 1986; Makino 1991) on GRAPE-5 (Kawai et al. 2000), a special-purpose computer designed to accelerate N-body simulations. For most simulations, we used the GRAPE-5 system at the Astronomical Data Analysis Center of the National Astronomical Observatory, Japan. We used the opening parameter $\theta = 0.4$ for the cosmological simulation and $\theta = 0.5$ for the halo simulation. The simulations presented below required, for example, in run L6, $\sim$80 s per time step, and thus one run (16k time steps) was completed in 370 CPU hr with a GRAPE-5 board connected to a host workstation with Alpha 21264 CPU (833 MHz).

TABLE 2
SIMULATION MODELS

Model	Run	M_v ($10^{14}\ M_\odot$)	r_v (Mpc)	N_v	m ($10^8\ M_\odot$)	Δt (10^6 yr)	N
SCDM	S1	8.67	2.62	1,676,525	5.17	1.57	5,074,432
	S2	5.46	2.21	1,056,312	5.17	1.57	3,523,844
	S3	3.68	1.97	1,421,930	2.58	1.57	3,478,480
	S4	3.58	1.91	1,383,674	2.58	1.57	4,104,120
LCDM.....	L1	7.83	2.34	1,288,779	6.08	0.82	3,624,848
	L2	5.32	2.08	875,058	6.08	1.63	4,360,512
	L3	3.97	1.85	1,306,187	3.04	0.82	3,066,944
	L4	2.17	1.52	1,425,526	1.52	0.82	3,536,640
	L5	2.15	1.52	707,569	3.04	1.63	2,058,140
	L6	1.83	1.43	1,809,105	1.01	0.82	5,458,688
OCDM	O1	8.58	2.34	1,411,523	6.08	0.68	3,711,232
	O2	4.27	1.86	702,022	6.08	1.37	1,748,480
	O3	2.18	1.47	717,056	3.04	1.37	2,148,736

3. RESULTS

3.1. *Snapshots*

Figure 1 shows the particle distribution for all runs at $z = 0$. The length of the side for each panel is equal to $2r_v$. For these plots, we shifted the origin of coordinates to the position of the potential minimum. In Table 2, we summarized the radius r_v, the mass M_v, and the number of particles N_v within r_v at $z = 0$.

3.2. *Density Profile*

Figure 2 shows the density profiles for all runs at $z = 0$. For run O2, we plot the density profile at $z = 0.026$ because the merging process occurs just near the center of halo at $z = 0$. The position of the center of the halo was determined using the potential minimum, and the density is averaged over each spherical shell, whose width is $\log_{10}(\Delta r) = 0.0125$. For illustrative purposes, the densities are shifted vertically.

In this figure, we plot the densities in the thick lines if the two criteria introduced in Paper I: (1) $t_{\rm rel}(r)/t > 3$ and (2) $t_{\rm dyn}(r)/\Delta t > 40$ are satisfied, where $t_{\rm rel}(r)$ is the local two-body relaxation time and $t_{\rm dyn}(r)$ is the local dynamical time. This means that the densities in the central region plotted in the thin lines are influenced by the numerical artifacts (mainly two-body relaxation), and they are not reliable. In

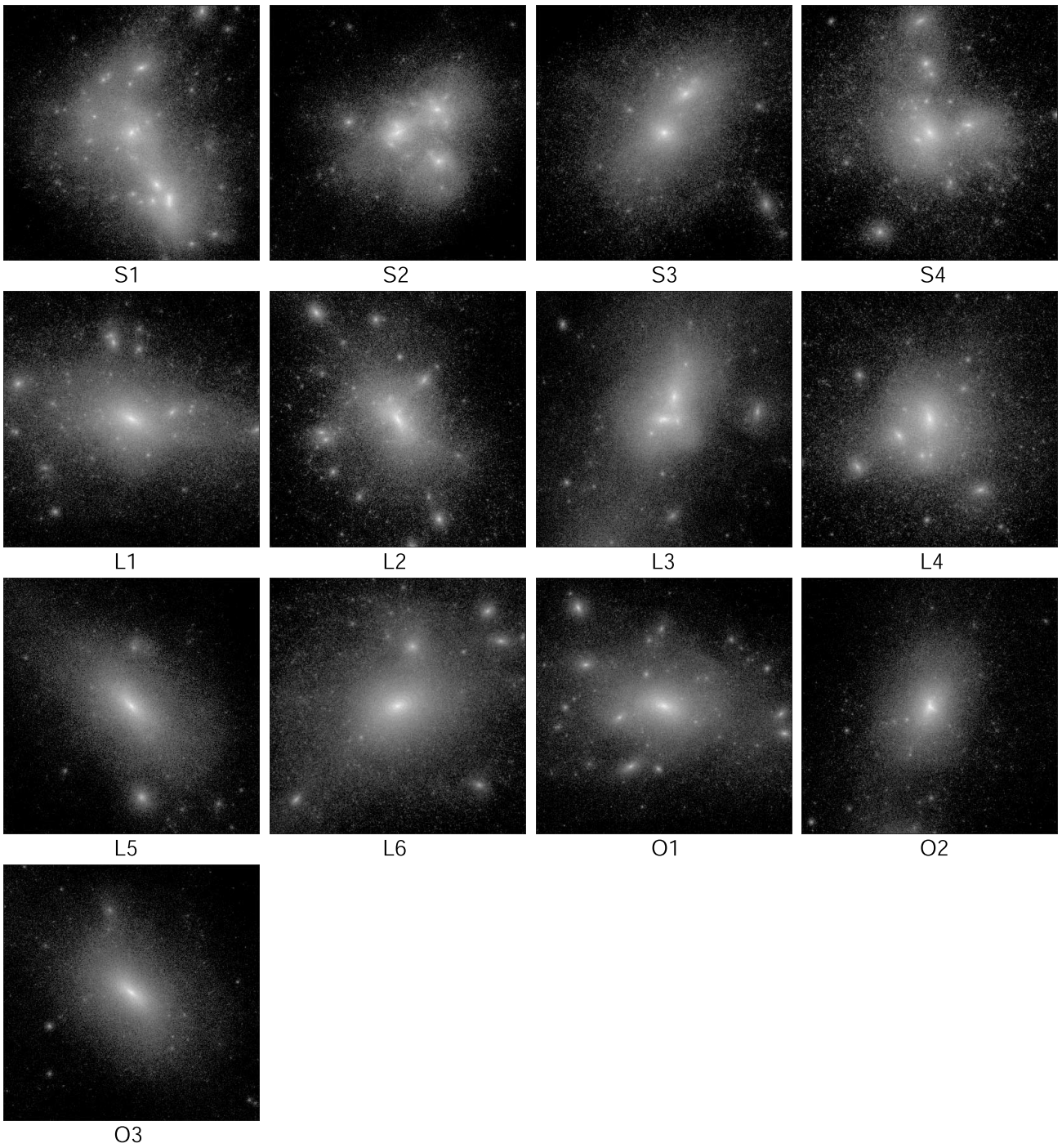

FIG. 1.—Snapshots from all runs at $z = 0$. The length of the side for each panel is equal to $2r_v$.

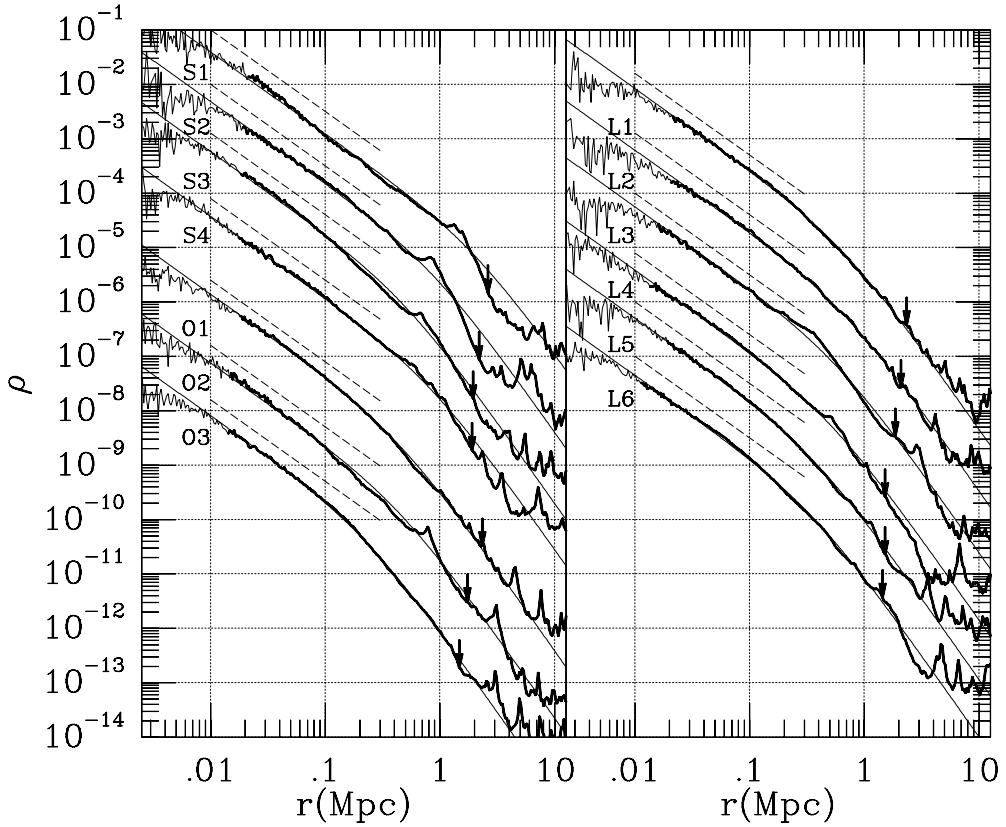

FIG. 2.—Density profiles of the halos for all runs at $z \simeq 0$. Only the densities plotted in the thick lines satisfy the accuracy criteria in § 3.2. Those plotted in the thin lines are influenced by numerical artifacts. The unit of density is $M_\odot$ pc^{-3}. The labels on the left of the profiles indicate the run name. The profiles except for runs S1 are vertically shifted downward by 1, 2, 3, 5, 6, and 7 dex for runs S2, S3, S4, O1, O2, and O3 and by 1–6 dex for runs L1–L6, respectively. The arrows indicate r_v. The thin dashed lines indicate the densities proportional to $r^{-1.5}$. The thin solid curves indicate the density profile given by eq. (2) (the M99 profile).

the following discussion, we only use the densities plotted in the thick lines.

In all runs we can see that the central density cusps are approximately proportional to $r^{-1.5}$. In other words, the power of the cusp is -1.5 and is independent of the cosmological models we simulated. The shallowing of the power-law index of the inner cusp observed in the LCDM runs by Jing & Suto (2000) was not reproduced in our LCDM runs.

Moreover, the density profiles are in good agreement with the profile given by equation (2) (the M99 profile) in all runs. The fitting was done using M_v and the least-squares fit of $(\rho - \rho_{\rm M99})/\rho_{\rm M99}$ at $r < 0.5$ Mpc. We obtained the scale radii r_0 as 2.08, 0.90, 0.49, and 0.84 Mpc for the S1–S4 runs, 0.67, 0.67, 0.58, 0.52, 0.38, and 0.37 Mpc for the L1–L6 runs, and 0.43, 0.45, and 0.23 Mpc for the O1–O3 runs. The agreement is very good for the inner region. In the outer region the agreement is not very good, simply because the outer profile shows large fluctuations caused by individual infalling halos. The agreement in outer region is better in the LCDM and OCDM models than in the SCDM model. This is because the halo in the LCDM and OCDM models is typically formed earlier, and it is dynamically quiet around $z \sim 0$.

Figure 3 shows the scale densities of the profile ρ_0 (eq. [2]) and the concentration parameter $c \equiv r_v/r_0$ as a function of total mass. These values in the S/LCDM models are consistent with those obtained by M99 and Jing & Suto (2000). We can see a tendency that cluster-sized halos in OCDM models are more compact than that of their S/LCDM counterparts of the same mass.

Figures 4, 5, and 6 show residuals, $(\rho - \rho_{\rm M99})/\rho_{\rm M99}$ and $(\rho - \rho_{\rm NFW})/\rho_{\rm NFW}$, for SCDM, LCDM, and OCDM models, respectively. The fitting procedure for the NFW profile is the same as that for the M99 profile. The degree of fitting to the NFW profile is worse than that to the M99 profile. Moreover, we can see that the sign of the residuals for the NFW model systematically changes around at 0.05 Mpc. This means the central slope of the NFW profile is too shallow for most models.

4. CONCLUSION AND DISCUSSION

We performed N-body simulations of dark matter halo formation in three CDM models: standard, lambda, and open. We simulated 13 halos whose mass range is $(1.8\text{–}8.6) \times 10^{14}\ M_\odot$. We used a widely adapted "resimulation" method to set up initial conditions of halos and include the external tidal field. We found that, in all runs and in our resolution limits, the final halos have density cusps proportional to $r^{-1.5}$, and the profiles show good agreement with the M99 profile, regardless of the cosmological models.

There are some claims that the innermost slope should converge not to $r^{-1.5}$ but to a shallower one (e.g., Taylor,

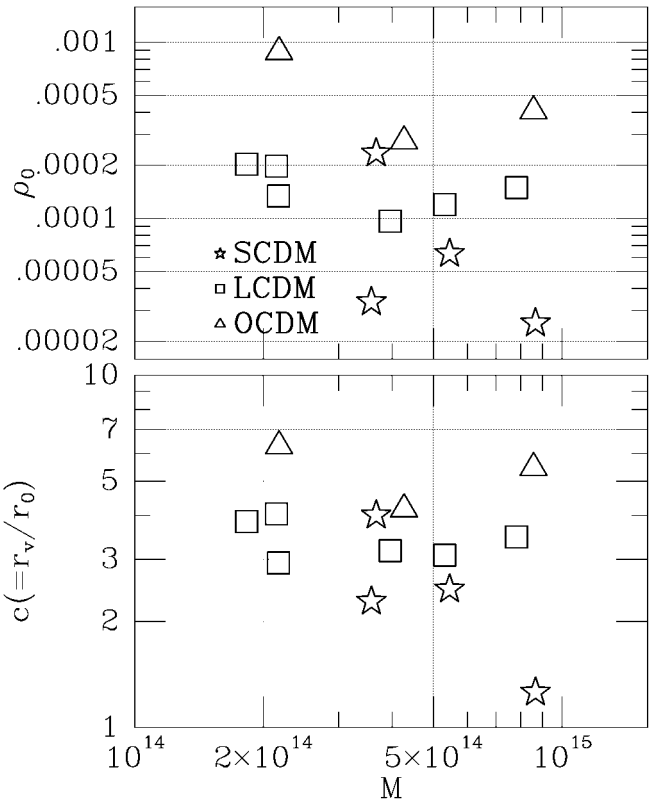

FIG. 3.—Scale density ρ_0 in the unit of $M_\odot$ pc^{-3} and concentration parameter $c = r_v/r_0$ as a function of total mass in solar mass. The star, square, and triangle symbols show those for the SCDM, LCDM, and OCDM models, respectively.

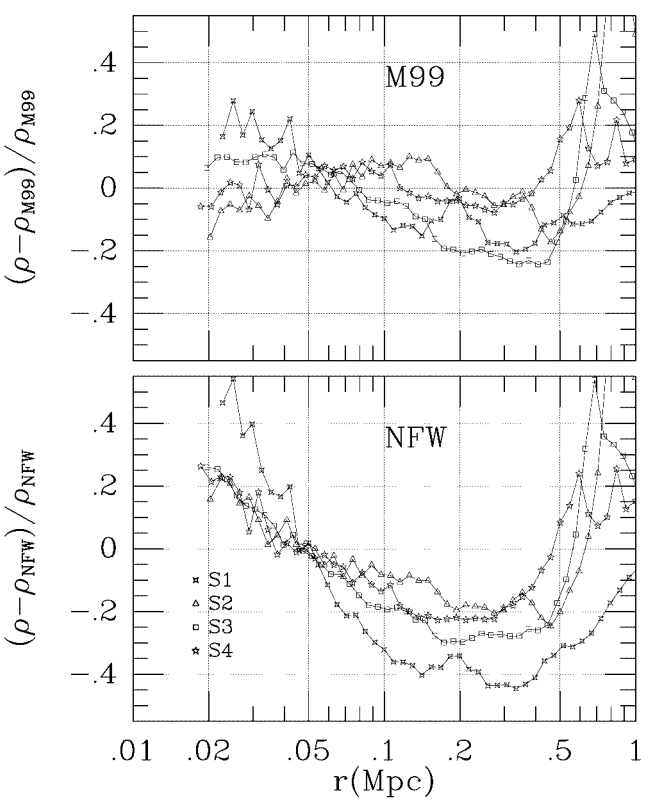

FIG. 4.—Residuals $(\rho - \rho_{NFW})/\rho_{NFW}$ and $(\rho - \rho_{M99})/\rho_{M99}$ as a function of radius for the SCDM model.

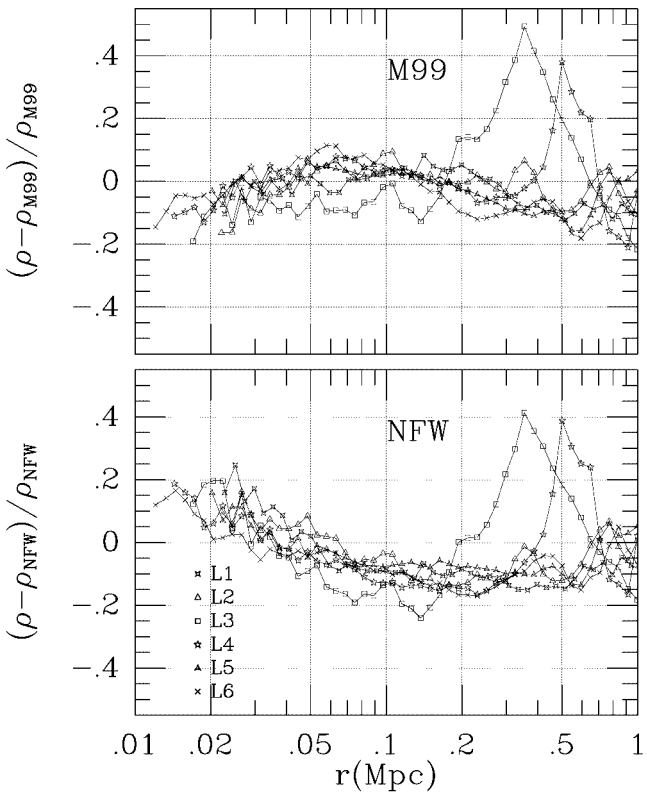

FIG. 5.—Same as Fig. 4, but for the LCDM model

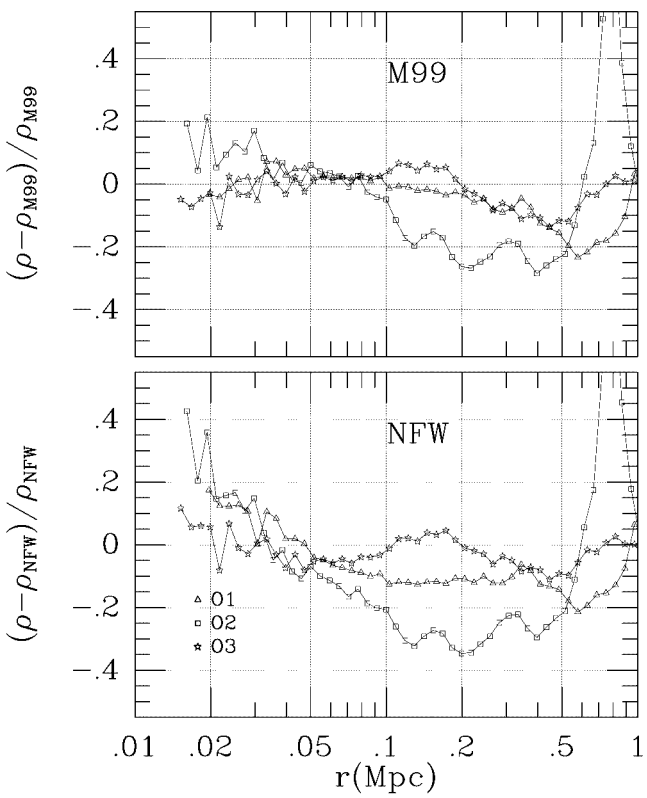

FIG. 6.—Same as Fig. 4, but for the OCDM model

Navarro 2001). Indeed, if we do not pay attention to numerical artifacts, we may see in our simulation results (Fig. 2) that the innermost slopes of all runs become shallower than -1.5. However, Figure 2 shows that the inner region where the slopes are shallower than $r^{-1.5}$ is not reliable, because in this region the accuracy criteria are not satisfied. The numerical artifact that makes the cusp shallower is mainly the two-body relaxation effect in this region (see Paper I). Therefore, we emphasize that discussions based on simulation results without careful analysis of the influence by the two-body relaxation effects are misleading.

In our LCDM run, we could not reproduce the shallowing of the power-law index of the inner cusp observed in the LCDM runs by Jing & Suto (2000). This difference could be due to the smoothing by two-body relaxation in their cluster-sized halos. In this paper, we show that the density profile within $\sim 0.01 r_{200}$ is smoothed by the two-body relaxation. The density at $0.01 r_{200}$ and the mass resolution in their cluster-sized halo are similar to those in ours. The density profile in their simulations within $0.01 r_{200}$, at which point the profile begins to depart from $r^{-1.5}$ inward, could be affected by the two-body relaxation. If their simulations had been performed with higher mass resolution, the slope might have approached -1.5. The tendency can be already seen in their galaxy-sized halo. All halos have the cusp proportional to $r^{-1.5}$ in their galaxy-sized halos, whose central densities at $0.01 r_{200}$ are almost similar to those of their cluster-sized run and mass resolutions are about 100 times higher.

Recently, Power et al. (2003) presented a set of convergence tests for numerical accuracy. In apparent contradiction to our results, they claimed to have found a shallower slope (-1.2) in their simulations, although they used accuracy criteria similar to ours. We are now carefully investigating the origin of the difference and will discuss it elsewhere.

Our results show that the NFW's claim concerning the universality is certainly valid. On the other hand, the density profiles obtained are not in agreement with the NFW profile at the central region. Although it is important to find the convergence slope by further simulations, a simple explanation would be required for our final understanding of the universal profile. At present, we do not fully understand why the profile is universal and/or why the power of central cusp is -1.5, which we will address in a future study.

We are grateful to Atsushi Kawai and Eiichiro Kokubo for their help in preparing the hardware and software environment of the GRAPE-5 system and to Yasushi Suto, Atsushi Taruya, and Masamune Oguri for many helpful discussions. We gratefully acknowledge the use of the initial condition generator in the publicly available code HYDRA (1995) developed by H. M. P. Couchman, P. A. Thomas, and F. R. Pearce. Most of the numerical computations were carried out on the GRAPE system at ADAC (the Astronomical Data Analysis Center) of the National Astronomical Observatory, Japan. This research was partially supported by the Research for the Future Program (JSPS-RFTP 97P01102) and by the Grants-in-Aid (14740127 and 13440058) of Japan Society for the Promotion of Science.

REFERENCES

Barnes, J. E., & Hut, P. 1986, Nature, 324, 446
Couchman, H. M. P., Thomas, P. A., & Pearce, F. R. 1995, ApJ, 452, 797
Eke, V. R., Cole, S., & Frenk, C. S. 1996, MNRAS, 282, 263
Fukushige, T., & Makino, J. 1997, ApJ, 477, L9 (FM97)
———. 2001, ApJ, 557, 533 (Paper I)
Fukushige, T., & Suto, Y. 2001, ApJ, 557, L11
Ghigna, S., Moore, B., Governato, F., Lake, G., Quinn, T., & Stadel, J. 2000, ApJ, 544, 616
Hoffman, Y., & Shaham, J. 1985, ApJ, 297, 16
Huss, A., Jain, B., & Steinmetz, M. 1999, MNRAS, 308, 1011
Jing, Y. P., & Suto, Y. 2000, ApJ, 529, L69
Kawai, A., Fukushige, T., Makino, J., & Taiji, M. 2000, PASJ, 52, 659
Kitayama, T., & Suto, Y. 1997, ApJ, 490, 557
Klypin, A., Kravtson, A. V., Bullock, J. S., & Primack, J. R. 2001, ApJ, 554, 903
Makino, J. 1991, PASJ, 43, 621
Moore, B., Governato, F., Quinn, T., Statal, J., & Lake, G. 1998, ApJ, 499, L5
Moore, B., Quinn, T., Governato, F., Statal, J., & Lake, G. 1999, MNRAS, 310, 1147 (M99)
Navarro, J. F., Frenk, C. S., & White, S. D. M. 1996, ApJ, 462, 563
———. 1997, ApJ, 490, 493 (NFW)
Power, C., Navarro, J. F., Jenkins, A., Frenk, C. S., White, S. D. M., Springel, V., Stadal, J., & Quinn, T. 2003, MNRAS, 338, 14
Syer, D., & White, S. D. M. 1998, MNRAS, 293, 337
Taylor, J. E., & Navarro, J. F. 2001, ApJ, 563, 483
Thomas, P., et al. 1998, MNRAS, 296, 1061